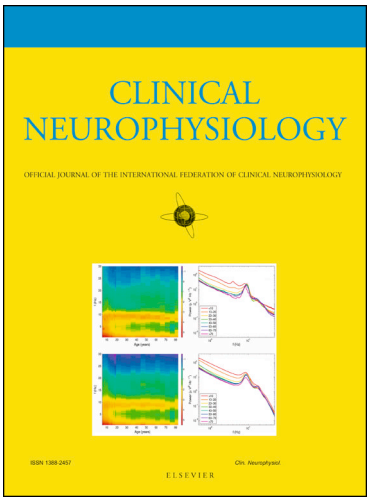

TMS-evoked long-lasting artefacts: a new adaptive algorithm for EEG signal correction

Elias P. Casula, Alessandra Bertoldo, Vincenza Tarantino, Michele Maiella, Giacomo Koch, John C. Rothwell, Gianna M. Toffolo, Patrizia S. Bisiacchi

PII: S1388-2457(17)30219-5
DOI: http://dx.doi.org/10.1016/j.clinph.2017.06.003
Reference: CLINPH 2008169

To appear in: *Clinical Neurophysiology*

Received Date: 2 February 2017
Revised Date: 8 June 2017
Accepted Date: 9 June 2017

Please cite this article as: Casula, E.P., Bertoldo, A., Tarantino, V., Maiella, M., Koch, G., Rothwell, J.C., Toffolo, G.M., Bisiacchi, P.S., TMS-evoked long-lasting artefacts: a new adaptive algorithm for EEG signal correction, *Clinical Neurophysiology* (2017), doi: http://dx.doi.org/10.1016/j.clinph.2017.06.003

TMS-evoked long-lasting artefacts: a new adaptive algorithm for EEG signal correction

Elias P. Casula[a,b,c], Alessandra Bertoldo[d], Vincenza Tarantino[b], Michele Maiella[a], Giacomo Koch[a], John C. Rothwell[c], Gianna M. Toffolo[c], Patrizia S. Bisiacchi[b]

[a] Non-invasive Brain Stimulation Unit, IRCCS Santa Lucia Foundation, Rome, Italy

[b] Department of General Psychology, University of Padua, Padua, Italy

[c] Sobell Department of Motor Neuroscience and Movement Disorders, University College London, London, United Kingdom

[d] Department of Information Engineering, University of Padua, Padua, Italy

Corresponding author:
Elias Paolo Casula
Santa Lucia Foundation, Via Ardeatina 306, 00142, Rome, Italy
Tel.: +39 3458499276
E-mail: elias.casula@gmail.com

Abstract

Objective: During EEG the discharge of TMS generates a long-lasting decay artefact (DA) that makes the analysis of TMS-evoked potentials (TEPs) difficult. Our aim was twofold: (1) to describe how the DA affects the recorded EEG and (2) to develop a new adaptive detrend algorithm (ADA) able to correct the DA.

Methods: We performed two experiments testing 50 healthy volunteers. In experiment 1, we tested the efficacy of ADA by comparing it with two commonly-used independent component analysis (ICA) algorithms. In experiment 2, we further investigated the efficiency of ADA and the impact of the DA evoked from TMS over frontal, motor and parietal areas.

Results: Our results demonstrated that (1) the DA affected the EEG signal in the spatiotemporal domain; (2) ADA was able to completely remove the DA without affecting the TEP waveforms; (3). ICA corrections produced significant changes in peak-to-peak TEP amplitude.

Conclusions: ADA is a reliable solution for the DA correction, especially considering that (1) it does not affect physiological responses; (2) it is completely data-driven and (3) its effectiveness does not depend on the characteristics of the artefact and on the number of recording electrodes.

Significance: We proposed a new reliable algorithm of correction for long-lasting TMS-EEG artifacts.

Keywords: TMS, EEG, artefact, ICA, detrend.

Abbreviations: TMS, transcranial magnetic stimulation; EEG, electroencephalography; DA, decay artefact; ADA, adaptive detrend algorithm; MEP, motor-evoked potential; TEP, TMS-evoked potential; MFG, middle frontal gyrus; M1, primary motor cortex; IPS, inferior parietal sulcus; ICA, independent component analysis; RMT, resting motor threshold; FDI, first dorsal interosseous; GMFP, global mean field power; TRSP, TMS-related spectral perturbation; TOI, time window of interest

Highlights

- TMS-evoked decay artefact (DA) makes the analysis of TMS-evoked potentials (TEPs) difficult.
- We developed a new adaptive algorithm (ADA) to correct DA in a completely data-driven way.
- Our study showed that ADA is able to completely remove the DA without corrupting the TMS-evoked physiological response.

1. Introduction

In the last twenty years, the combination of transcranial magnetic stimulation (TMS) and electroencephalography (EEG) has provided new insights into the investigation of brain dynamics (Ilmoniemi and Kičić, 2010). However, besides the potential of combining these two techniques, their simultaneous use produces different EEG artefacts of electrical and physiological nature. Electrical artefacts result from the voltage induced in the electrodes by the TMS pulse, which is several orders of magnitude larger than the physiological responses (Virtanen et al., 1999). Indeed, the TMS pulse produces a high-frequency spike of several mV of electric nature lasting a few milliseconds (Veniero et al., 2009). In addition, TMS results in a number of physiological EEG artifacts. First, a large bipolar spike peaking at 4-10 and 8-20 ms is produced by the stimulation of scalp muscles and is particularly evident when stimulating lateral areas (Korhonen et al., 2011; Mutanen et al., 2013). Moreover, TMS stimulation results in both auditory and somatosensory artifacts produced by the coil click and tactile sensation (Nikouline et al., 1999; Tiiitinen et al., 1999). Finally, a long-lasting artefact has been recently described by a few papers (e.g. Litvak et al., 2007; Rogasch et al., 2014) and termed decay artefact (DA). This artefact is characterized by a slow drift of the signal of a few electrodes (usually the ones underneath the stimulating coil) whose amplitude can vary from a few μV to tens of μV impeding the correct realignment to the baseline level for tens or hundreds of milliseconds after the TMS pulse (Rogasch et al., 2014; Hernandez-Pavon et al., 2012). The nature of the DA is still a matter of debate: some authors hypothesized that during the TMS pulse some currents can pass through the electrode-electrolyte interface causing a polarization and, consequently, an EEG baseline shift (Julkunen et al., 2008). Alternatively, it has been suggested that the artefact can be produced by the electromotive forces induced in the electrode wires (Sekiguchi et al., 2012) or from the scalp muscular activity evoked by the stimulation (Rogasch et al., 2014).

Throughout the years, several on-line and off-line strategies have been developed to deal with TMS-induced EEG artifacts of electrical and physiological nature. The progressive improvements in the amplifier technology have allowed the successful removal or reduction of the TMS pulse-induced artefact during the EEG recording (Ilmoniemi et al., 1997; Virtanen et al., 1999; Bonato et al., 2006). The on-line reduction of physiological artifacts is also possible. For instance, the use of an *ad-hoc* white noise masking the coil click minimizes the auditory artifacts (Massimini et al., 2005). Muscle artifacts can be reduced by varying the coil angle (Mutanen et al., 2013). Finally, somatosensory artifacts can be reduced by using a thick of a few millimeters to reduce the tactile sensation during the stimulation. Different off-line methods of correction have also been developed by using (1) a subtractive approach, in which a template artefact generated through a phantom (Bender et al., 2005) or a TMS control condition (Thut et al., 2003) is subtracted from the data; (2) independent component analysis (ICA) or principal component analysis (PCA) (e.g. Korhonen et al., 2011; Ter Braack et al., 2013; Metsomaa et al., 2014; Rogasch et al., 2014).

Despite these strategies have been successfully applied for the correction of most of the TMS-induced artefacts, their feasibility in removing the DA is problematic. Currently, an on-line correction for this artefact is still lacking. The most common off-line methods consist in (1) using a linear detrend function in order to realign the signal on the baseline level (e.g. Van der Werf et al., 2006; Zanon et al., 2010) or (2) removing the DA-related components by means of ICA or PCA (e.g. Korhonen et al., 2011; Ter Braack et al., 2013; Metsomaa et al., 2014; Rogasch et al., 2014). However, none of these solutions may be considered optimal. The linear detrend fits and subtracts a linear model to the drift assuming that the DA follows a linear trend, which is not always true, especially for the first part of the drift (Litvak et al., 2007). Indeed, the DA can follow a non-linear trend, so that the correction with a standard linear detrend might cause an uncompleted removal of the artefact or a distortion of the signal. ICA is a computational method for decomposing multivariate signals into additive independent non-gaussian signals, which has been successfully

applied to multi-channel EEG data (Onton et al., 2006). Although ICA has been used to correct muscle and blink artefacts produced by TMS (Hamidi et al., 2010; Korhonen et al., 2011; Hernandez-Pavon et al., 2012), it presents a number of limitations, discussed in the present manuscript.

In the present study we propose an adaptive detrend algorithm (ADA) able to discriminate the different trends of the DA (i.e. linear or non-linear) and to adaptively compute and subtract a different model to the drift. Specifically, when the DA does not follow a linear trend, ADA computes a bi-exponential model to adequately describe the kinetics of the decay that generally shows to be the sum of two different patterns, i.e. a fast component in the initial phase and a slower component in the second part (Litvak et al., 2007). We performed two experiments: in experiment 1, we tested the efficacy of ADA in removing the DA evoked from TMS applied over M1 of a large sample of healthy volunteers (forty). We chose to stimulate M1 since the TMS-evoked potentials (TEPs) pattern over this area has been highly characterized by several studies. To test the efficacy of our algorithm, we compared the ADA-corrected signal with two common ICA algorithms, namely fastICA and INFOMAX. In experiment 2, we further tested the stability and reliability of ADA in removing the DA evoked from TMS of two other brain areas, namely the left middle frontal gyrus (MFG) and the left intraparietal sulcus (IPS).

2. Methods

2.1 Participants and procedure

Fifty right-handed healthy volunteers (27 females, mean age 24±4 years) were enrolled for this study after giving written informed consent. All participants were tested for TMS exclusion criteria (Rossi et al., 2009). The experimental procedure was approved by the Local Institutional Review Board, and was in accordance with the Declaration of Helsinki (Sixth revision, 2008). In experiment 1, forty participant underwent a TMS block of stimulation consisting of 80 single-pulses delivered over the left M1 during multichannel EEG recordings. In experiment 2, ten participants received three TMS blocks over the left M1, MFG and IPS. Throughout the entire session participants were seated on a comfortable armchair in front of a monitor at 80 cm of distance. They were asked to fixate a white cross (6×6 cm) in the middle of a black screen, in order to avoid eye movements during the EEG recordings, and to maintain a relaxed position. During TMS participants wore in-ear plugs which continuously played a white noise that reproduced the specific time-varying frequencies of the TMS click, in order to mask the click and avoid possible auditory ERP responses (Massimini et al., 2005). The intensity of the white noise was adjusted for each participant by increasing the volume (always below 90 dB) until the participant was sure that s/he could no longer hear the click (Paus et al., 2001). To reduce the bone-conducted sound and the tactile sensation we used an EEG cap with a 4 mm plastic sheet that reduced the transmission of mechanical vibration produced by the coil (Nikouline et al., 1999).

2.2 Transcranial Magnetic Stimulation (TMS)

TMS was carried out using a Magstim R^2 stimulator with a 70mm figure-of-eight coil (Magstim Company Limited, Whitland, UK), which produced a biphasic waveform with a pulse width of ~0.1 ms. For M1 stimulation, the position of the coil on the scalp was functionally defined as the site in which TMS evoked the largest MEPs in the relaxed first dorsal interosseous (FDI) muscle of

the right hand. For MFG and IPS stimulation, we based on the 10-20 system, stimulating the F3 and P3 electrode, respectively. For M1 and MFG stimulation, the coil was oriented tangentially to the scalp at about 45° angle away from the midline. For IPS stimulation, the coil was oriented at about 15° angle toward the midline. To ensure the same stimulation conditions during the entire experiment, coil positioning and orientation on the optimal hotspot were constantly monitored by means of the Brainsight neuronavigation system (using the ICBM152 template), coupled with a Polaris Vicra infrared camera (NDI, Waterloo, Canada). Stimulation intensity was set at 90% of the resting motor threshold (RMT), defined as the lowest TMS intensity which evoked at least five out of ten MEPs with an amplitude > 50 μV peak-to-peak in the contralateral FDI at rest (Rossini et al., 1994). Single-pulses were delivered with an inter-stimulus interval (ISI) of 4-6 seconds. Surface EMG was acquired from the right FDI muscle via Ag/AgCl electrodes in a belly-tendon montage (Myohandy Matrix Line – Micromed Srl, Mogliano Veneto, Italy). Raw signals were sampled at 2.5 kHz and band-pass filtered at 50-1000 Hz.

2.3 Electroencephalographic recordings (EEG) and pre-processing

To test the reliability of ADA with different TMS-EEG setups, we recorded EEG using two TMS-compatible amplifiers (Micromed SD MRI, Micromed Srl., Mogliano Veneto, Italy in experiment 1; Advanced Neuro Technology, Enschede, Netherlands in experiment 2) connected to 29 (experiment 1) or 60 (experiment 2) TMS-compatible Ag/AgCl pellet electrodes. EEG signal was online filtered at 0.1-500 Hz with a sampling frequency of 2048 Hz. Recordings were referenced to AFz electrode, the ground electrode was placed on POz. In order to reduce TMS-induced artefacts we kept the skin impedance below 5 kΩ (Julkunen et al., 2008). Off-line analysis was performed with EEGLAB 13.3.2 (Delorme and Makeig, 2004) and Fieldtrip toolbox (Oostenveld et al., 2010), running in a MATLAB environment (Version 7.9.0, MathWorks Inc., Natick, USA). We first removed the TMS-pulse artefact by applying a cubic interpolation from 1 ms before to 15 ms after the TMS pulse. The continuous EEG signal was then band-pass filtered between 1 and 80 Hz (Butterworth zero-phase

filters). A 50 Hz notch filter was also applied to reduce noise from electrical sources. After this, the continuous EEG signal was segmented into epochs starting 500 ms before the TMS pulse and ending 500 ms after it. A baseline correction taken as 500 ms before the TMS pulse was applied on all the epochs, which were subsequently visually inspected and those excessively noisy excluded from the analysis (resulting less than 5% for each participant). A first INFOMAX ICA was run to identify components reflecting the artifacts not directly related to TMS (i.e. eye blinks, muscle activity). The identified components were visually inspected in terms of scalp distribution, frequency, timing and amplitude and then removed. None of the components related to the DA were removed at this point. These were subsequently removed by means of either the ADA (see methods section 2.4) or two different ICA algorithms (INFOMAX and FASTICA), separately performed for each participant's EEG dataset. The criteria to define an ICA component as related to the DA were:

- *Waveform*, i.e., the signal showed a typical slow trend (Rogasch et al., 2014), starting from a few ms after the TMS pulse to at least 30 ms;
- *Temporal distribution*, i.e., the decay trend emerged in at least 75% of the trials;
- *Spatial distribution*, i.e., ICs were topographically distributed around the stimulated site.

Components that satisfied all the three criteria were considered related to the DA and then removed. To verify the reliability of our identification procedure, this was separately performed by two experimenters (EPC and VT). At the end of the EEG pre-processing we had three conditions for each participant's EEG dataset: an EEG signal with no correction of the DA (RAW condition); an EEG signal corrected with ICA (ICA condition) and an EEG signal corrected with ADA (ADA condition). The same pre-processing steps were applied for the two experiments. At the end of the pre-processing stage, in experiment 2, we re-referenced the signal to the average of all the electrodes.

2.4 Adaptive detrend algorithm (ADA)

The algorithm script was developed in MATLAB. As a first step, for each channel, the epoched EEG signal in the interval 15-500 ms after TMS, $z_{(15-500)}(t)$, was modeled using a regression line,

$$(1)\ z_{(15-500)}(t) = m \cdot t + q$$

where *t* denotes time and [*m*, *q*] the model parameters to be estimated. Subsequently, a two-exponential function was used,

$$(2)\ z_{(15-500)}t = A_1 \cdot \exp(a_1 t) + A_2 \cdot \exp(a_2 t)$$

where $[A_1, a_1, A_2, a_2]$ are the four model parameters. Parameters [*m*, *q*], of the regression line were estimated by weighted linear least squares, while for the two-exponential function the weighted non-linear least squares were used [*A1*, *a1*, *A2*, *a2*]. Weights were chosen optimally, i.e., proportional to the inverse of the (constant) variance of the measurement errors assumed to be additive, uncorrelated, gaussian, zero mean (Cobelli et al., 2000). To make a selection between the two functions in term of model parsimony, the Akaike information criterion (Akaike, 1979) was used,

$$(3)\ AIC = Nlog(WRSS) + 2 \cdot P$$

where *WRSS* is the weighted residual sum of squares (i.e. the weighted sum of the squares of the difference between acquired data and predicted values), *P* is the number of parameters (i.e. 2 for the regression line, 4 for the two-exponential function) and *N* is the number of the data points used to fit the functions. The function having the lowest AIC value was selected as the best to describe the DA and used to correct the acquired signal as,

$$(4)\ z^{correct}_{(15-500)}(t) = z^{acquired}_{(15-500)}(t) - z^{best\ model}_{(15-500)}(t)$$

2.5 Time-domain EEG analyses

To assess the cortical response induced by TMS over all the scalp, we used multiple dependent t-tests comparing TEP waveform at each electrode from 100 ms before to 500 ms after the TMS pulse. A non-parametric, cluster-based permutation statistics was conducted to correct for multiple comparisons. This method performs a non-parametric statistical test by calculating the Monte Carlo estimate of the significance probabilities from surrogate distributions constructed by randomly permuting the original conditions data for 3000 times. The clusters for permutation analysis were defined as the two (or more) neighboring electrodes in which the t-value at a given time point exceeded a threshold of $p<0.05$. The electrodes and the time windows within which the corrected signals significantly differed from the RAW uncorrected signal, were used to compute the TEPs peak-to-peak amplitude and latency for each condition (i.e. RAW, ICA corrections, ADA). Importantly, the peak-to-peak measure allowed us to compare the relative amplitude and latency of the TEPs regardless the baseline shift caused by the DA. The TEPs amplitudes and latencies were compared among conditions by means of a repeated-measures ANOVA with condition, TEP and electrode as within-subject factors. We performed two separate ANOVAs for INFOMAX and FASTICA correction. Sphericity of data was tested with the Mauchly's test; when sphericity was violated (i.e. Mauchly's test < 0.05) the Greenhouse-Geisser correction was used. *Post-hoc* comparisons were corrected by the Bonferroni method. To assess the cortical response induced by TMS at a global level, we computed the global mean field power (GMFP) considering a time window from 100 ms before (considered as a baseline) to 500 ms after stimulation (Lehmann and Skrandies, 1980). GMFP was computed as:

$$GMFP(t) = \sqrt{\frac{[\sum_i^k (V_i(t) - V_{mean}(t))^2]}{K}}$$

Where *t* is time, *K* the number of channels, V_i the voltage in channel *i* averaged across participants and V_{mean} is the mean of the voltage in all the channels.

2.6 Time/Frequency-domain EEG analysis

Analysis in the time/frequency domain were conducted in epochs starting 500 ms before to 500 ms after the TMS pulse in a frequency range starting from 4 to 45 Hz. We first performed a time/frequency decomposition for each epoch based on Morlet wavelet, than we computed TMS-related spectral perturbation (TRSP; Delorme and Makeig, 2004; Casula et al., 2016a) as:

$$TRSP(f,t) = \frac{1}{n}\sum_{k=1}^{n} |F_k(f,t)|^2$$

Where, for *n* trials, the spectral estimate *F* was computed at trial *k*, at frequency *f* and time *t*. TRSPs were baseline-normalized by subtracting the mean baseline log power spectrum in each trial from each spectral estimate. Significant deviations from baseline power were computed with a bootstrap method comparing for 200 times a surrogate data distribution of spectral estimates randomly selected within the baseline time window (i.e. from 400 ms to 100 ms before the TMS pulse) for each epoch, and then averaging them. To assess the effects of the DA in the time/frequency domain, we used multiple dependent t-tests comparing the uncorrected RAW data with the corrected data at F3, C3 or P3 electrode from 15 to 300 ms after TMS of MFG, M1 or IPS, respectively. To correct for multiple comparisons we used the false discovery rate method.

3. Results

3.1 Experiment 1: decay artefact

The identification and removal procedures of the DA-related ICA components separately conducted by two experimenters did not differed (p>0.05). We removed 3±1.3 components in the INFOMAX condition; 3±1 in the FASTICA condition. All the removed components presented the three criteria reported in methods section 2.3. In the ADA condition, the correction of the DA was performed by applying the two-exponential model in 82% of the trials. Figure 1 depicts the butterfly charts of the grand-average waveforms with the topographic voltage distribution at specific time points corresponding to the peaks of EEG activity. A clear DA is observable in the uncorrected data (RAW condition; fig. 1a): three electrodes (C3, FC1, and CP1) showed a positive decay artefact with maximum amplitude of ~5 (CP1), ~9 (C3) and ~15μV (FC1), lasting for about 400 ms (CP1) or more (FC1, C3). Notably, these electrodes were the closest to the site of stimulation. A strong negative shift of the signal was also appreciable in two electrodes of the hemisphere contralateral to the stimulation (FC2, Cz), although in this case the signal seems to realign to the baseline level at around 150 ms from the TMS pulse. Scalp maps of the voltage distribution (fig. 1a) showed a clear dipole over the site of stimulation. Specifically, the area around the site of stimulation, comprising the electrodes C3, FC1 and CP1, showed a sustained positivity lasting for more than 400 ms after the TMS pulse, which represents the DA in these electrodes. The negative shift observed over a few electrodes of the contralateral hemisphere was also observable until 100-150 ms from the TMS pulse. Such dynamic seems to be partially reduced after the INFOMAX and FASTICA corrections even if a positive DA was still present at 400 ms over the site of stimulation in both conditions (fig. 1c,d). After the ADA correction (fig. 1b) the channels were realigned to a standard range of amplitude (from +4 to -6 μV) no evoked activity was visible from 280 ms after the TMS pulse, as usually reported (Paus et al., 2001; Kommsi et al., 2002; Bender et al., 2005; Bonato et al., 2006; Lioumis et al., 2009; Ferreri et al., 2011; Veniero et al., 2013). At 400 ms from the TMS pulse the voltage distribution on the scalp was around 0 μV.

3.2 Experiment 1: TMS-evoked potentials distribution

Single-pulse TMS over M1 evoked a well-known pattern of positive and negative deflections lasting up to 250-280 ms, comprising the following peaks: P30, N45, P55, N100 and P180 (Paus et al., 2001; Kommsi et al., 2002; Bender et al., 2005; Bonato et al., 2006; Lioumis et al., 2009; Ferreri et al., 2011; Veniero et al., 2013; Casula et al., 2016a; Premoli et al., 2014). Such pattern of response was observable in all the electrodes and it appeared more pronounced nearby the site of stimulation, as previously reported (Paus et al., 2001; Kommsi et al., 2002; Bender et al., 2005; Bonato et al., 2006; Lioumis et al., 2009; Ferreri et al., 2011; Veniero et al., 2013; Casula et al., 2016b; 2017). From a visual inspection, the TEP waveforms did not appear to be corrupted by the different artefact corrections (fig. 1). However, the influence of the DA over the scalp maps of voltage distribution is clear in the RAW signal and, to some extent, after the INFOMAX and FASTICA corrections (fig. 1a,c,d). A well-known TEP distribution was observable after the ADA correction (fig. 1b): the earlier TEPs were distributed over the site of stimulation (P30) and on the contralateral fronto-central regions (N45), whereas the later TEPs had a large distribution over the stimulated hemisphere (P55) and a bilateral distribution over the central (N100) and fronto-central areas (P180), as previously reported (Bonato et al., 2006; Ferreri et al., 2011; Veniero et al., 2013; Premoli et al., 2014; Casula et al., 2016b; 2017).

3.3 Experiment1: TMS-evoked potentials amplitude

To assess "where" (i.e. in which electrode) and "when" (i.e. in which temporal window) the DA corrections significantly affected the signal, we applied a cluster-based permutation analysis (see methods section 2.5) comparing the uncorrected RAW data with the corrected data (i.e. INFOMAX, FASTICA and ADA). The analysis revealed that TEPs showed significant differences in amplitude across conditions in the following time windows (all Monte Carlo ps < 0.05; fig. 2):

- RAW *vs.* INFOMAX: 16-250 ms in FC1; 21-60 ms and 67-250 ms in CP1;

- RAW *vs.* FASTICA: 16-250 ms in FC1, CP1 and C3;
- RAW *vs.* ADA: 16-250 ms in FC1, CP1, C3.

To assess "how much" the artefact corrections affected the TEPs we compared the peak-to-peak amplitude and latency of the components within the temporal window detected as significant, by means of repeated-measures ANOVA. We performed two analyses comparing the RAW uncorrected data with ICA and ADA procedures.

3.3.1 Analysis 1: RAW vs. INFOMAX vs. ADA

In this analysis we performed a 3×4×2 repeated-measures ANOVA with condition (RAW *vs.* INFOMAX *vs.* ADA), TEP (P30/N45, N45/P55, P55/N100, N100/P180) and electrode (FC1, CP1) as within-subjects factors. The analysis of TEP amplitude revealed a significant condition×TEP×electrode interaction [$F(2.9,104.9) = 8.55$, $p < 0.001$]. In the FC1 electrode, *post-hoc* analysis of the interaction revealed a significantly higher amplitude of three TEPs (N45/P55, P55/N100, N100/P180) in the INFOMAX condition compared to the RAW (N45/P55: 2.412±0.54 µV, $p < 0.001$; P55/N100: 1.959±0.69 µV, $p = 0.022$; N100/P180: 1.731±0.69 µV, $p = 0.05$), two of these components (N45/P55 and P55/N100) were also significantly higher in the INFOMAX condition compared to the ADA (N45/P55: 2.566±0.58 µV, $p < 0.001$; P55/N100: 2.717±0.68 µV, $p = 0.001$) (fig. 3). In the CP1 electrode, *post-hoc* analysis of the interaction revealed a significantly higher amplitude of the N45/P55 component in the INFOMAX condition compared to the RAW (1.071±0.43 µV, $p = 0.05$) and to the ADA condition (1.080±0.43 µV, $p = 0.05$) (fig. 3). No TEP differences were detected between the ADA and the RAW condition in any of the electrodes (all ps > 0.05).

3.3.2 Analysis 2: RAW vs. FASTICA vs. ADA

In this analysis we performed a 3×4×3 repeated-measures ANOVA with condition (RAW *vs.* FASTICA *vs.* ADA), TEP (P30/N45, N45/P55, P55/N100, N100/P180) and electrode (FC1, C3, CP1) as within-subjects factors. The analysis on the TEPs amplitude revealed a significant condition×TEP×electrode interaction [$F(4.6,163.1) = 9.54$, $p < 0.001$]. In the FC1 electrode, post-hoc analysis of the interaction revealed a significantly lower amplitude of the P30/N45 component in the FASTICA condition compared to the RAW (2.380±0.49 μV, $p < 0.001$) and to the ADA condition (1.804±0.47 μV, $p = 0.001$) (fig. 3). In the CP1 electrode, post-hoc analysis of the interaction revealed a significantly lower amplitude of the N100/P180 component in the FASTICA condition compared to the RAW condition (0.722±0.28 μV, $p = 0.045$) (fig. 3). In the C3 electrode, post-hoc analysis of the interaction revealed a significantly lower amplitude of the P55/N100 component in the FASTICA condition compared to the RAW (1.231±0.48 μV, $p = 0.047$) and to the ADA condition (1.324±0.45 μV, $p = 0.017$); a significant lower amplitude of the N100/P180 component in the FASTICA condition compared to the RAW condition was also revealed (1.282±0.31 μV, $p = 0.001$) (fig. 3). Again, no TEP differences were detected between the ADA and the RAW condition in any of the electrodes (all ps > 0.05).

3.4 Experiment 2: decay artefact

The identification procedures of the DA-related ICA components separately conducted by two experimenters did not differed ($p > 0.05$). Figure 4 depicts some examples of ICA components reflecting both linear and non-linear trends of the DA. All the DA-related ICA components presented the three criteria specified in methods section 2.3 and subsequently removed. Figure 5, 6 and 7 depicts the TEPs evoked from MFG, M1 and IPS before and after ADA correction. The DA is clearly observable in the RAW data for the first 500 ms after stimulation nearby the stimulated area: F1, F3, F5, FC3, FC5 after MFG stimulation; C1, C3, C5, FC1, FC3, FC5 after M1 stimulation; P1, P3, P5, CP1, CP3, C1 after IPS stimulation. The mean amplitude of the DA (MFG: 9.59±2.48 μV;

M1: 8.79±6.26 μV; IPS: 7.02±1.51 μV) did not differed among the three areas [F(1.19, 10.75)=1.19, p=0.31, ε=.117]. The correction of the DA was performed by applying the two-exponential model in 80% of the time.

3.5 Experiment 2: time/space-domain analysis

The cortical activity relative to the RAW condition as well as that one reconstructed after removing the DA using ADA is displayed in figure 5 (MFG stimulation), 6 (M1 stimulation) and 7 (IPS stimulation). As previously observed in experiment 1, scalp maps of voltage distribution in the RAW uncorrected data, showed a dipole over the stimulated area that masked the real TEPs distribution. This dynamic was observable over the three stimulated areas. Cluster-based analysis revealed that the DA was prominent over the electrodes surrounding the stimulated areas, but also in contralateral electrodes when stimulating MFG (figure 5) and IPS (figure 7). In the ADA corrected data, scalp maps of voltage distribution revealed an initial activity (15-40 ms after TMS) focused over the stimulated area, which subsequently spread bilaterally over central and posterior regions (50-250 ms after TMS). This dynamic is appreciable over the three areas of stimulation.

3.6 Experiment 2: time/frequency-domain analysis

Figure 8 depicts the TMS-evoked oscillatory activity locally, i.e., over the closest electrode to the stimulated area (i.e. F3 for MFG, C3 for M1 and P3 for IPS), and overall the scalp. Analysis on the TMS-evoked oscillatory activity did not reveal any significant difference between the RAW and the ADA condition in any of the frequency band considered (all ps>0.05).

4. Discussion

The aims of the present study were: (1) to develop a new algorithm for the offline correction of the DA that overcomes the intrinsic limitations of the commonly used methods of correction and (2) to investigate the impact of the DA generated by TMS pulse on the EEG signal. In the first experiment we evaluated the efficacy of ADA in removing the DA in a large sample size of healthy volunteers. In experiment 2, we investigated the effects of the DA and of its removal over three different brain areas. Overall, the results showed that (1) ADA succeed in removing the artefact, as revealed by the analyses in the time, space and frequency domain; (2) ADA did not affect the physiological responses, as revealed by the results of experiment 1 and (3) the DA significantly affected the EEG signal in the time and in the space domain.

The impact of the DA on the TMS-induced physiological responses is still a relatively unknown topic in literature. The present results demonstrated that the DA dramatically corrupted the TMS-evoked response both in the time and in the space domain. Indeed, the strong baseline shift caused by the DA produced a dipole in the scalp voltage maps over the site of stimulation for more than 400 ms after the TMS pulse, which masked the real distribution of the TEPs. Interestingly, this dynamic was clearly observable stimulating different areas. In addition, it seems that when stimulating MFG and IPS, the DA was stronger and affected not only the electrodes surrounding the site of stimulation, but also the contralateral ones. This might be due to the TMS-evoked muscular artifacts which are activated during the stimulation of frontal, temporal or parietal cranial muscles, resulting in larger DA artifacts. Along the same lines, a strong correlation between the DA and TMS-evoked muscular artifacts has been recently reported (Rogasch et al., 2014). Nevertheless, we did not find any difference in the DA amplitude among the three stimulated areas. Importantly, we found that the DA did not affect the TEP waveforms, as previously reported (Zanon et al., 2010; Hernandez-Pavon et al., 2012; Rogasch et al., 2014).

Correcting the DA represents a serious problem in the current TMS-EEG literature. In the present study we found that the trend of the DA was non-linear for more than 80% of the trials,

demonstrating the unsuitableness of a linear detrend as a method of correction. An alternative common procedure consists in interpolating the electrodes affected by the DA. However, this solution poses two main problems: firstly, the electrodes mostly affected by the DA are those below the site of stimulation, where the induced cortical responses are stronger, so the interpolation might lead to a substantial loss of information. Secondly, even the interpolating electrodes surrounding the affected ones usually are at least partially affected by the DA, making the interpolation problematic or inefficient. Currently, ICA is the most common solution for correcting the DA. However, even this solution presents a number of intrinsic limitations. A first critical point is that the criteria of identification and removal of the ICA components artefact-related are rarely specified in TMS-EEG papers, making such procedure too arbitrary and dependent from the experimenter's decisions. To our knowledge, only one published study tried to reduce this problem for TMS-EEG artifacts (i.e. Korhonen et al., 2011). These authors presented a new semi-automatic procedure, called enhanced deflation method, able to automatically detect and remove artefactual components basing on their characteristics. Such technique, although more robust compared to the manual method, is still preliminary due to the very small number of dataset tested. Another critical point is that ICA may also affect the physiological responses evoked by TMS (Ter Braack et al., 2013; Rogasch et al., 2014). Nevertheless, as far as we know, a direct investigation of the impact of ICA on physiological responses to TMS is still lacking. In our study, we tried to optimally apply ICA by establishing some strict criteria to identify the DA-related components, by using two common ICA algorithms, namely INFOMAX and FastICA. The identification of the DA-related ICA components did not differed between the experimenters, proving that our identification procedure was stable and reproducible and supporting previous studies that showed the feasibility of DA identification with ICA (Rogasch et al., 2014). Our results revealed that, after ICA correction, the peak-to-peak amplitude of the TEPs was significantly different from both the RAW and ADA conditions. Specifically, INFOMAX correction produced higher amplitude in 4 out of 8 TEPs, whereas FASTICA produced lower amplitude in 4 out of 12 TEPs. These differences are likely to be

produced by a corruption of the physiological responses caused by ICA correction, since the DA does not corrupt the TEP waveform *per se* (Zanon et al., 2010; Hernandez-Pavon et al., 2012; Rogasch et al., 2014). Notably, we did not find any difference in TEP amplitude between the ADA and the RAW condition. It must be taken in consideration that in the present study we identified (and subsequently removed) only the components that were clearly related to the DA (Rogasch et al., 2014); thus, it cannot be excluded that the removal of further components could have produced a stronger removal of the DA. However, this would pose two critical problems: first, the difficulty in establishing some clear criteria to identify the DA-related ICA components, making their choice too arbitrary; second, and more important, the removal of further components could have caused a stronger modification of the TEPs amplitude (Ter Braack et al., 2013). Indeed, we found that the highest difference in TEP amplitude were observable in the datasets where the number of removed components was higher (i.e. 4-6).

The second and main aim of the study was to develop an algorithm with the following characteristics: (1) that is able to correct the DA in an "adaptive way", i.e. that is able to discriminate and adapt the correction to the different trends and characteristics of the artefact (linear and non-linear); (2) that does not affect the physiological responses, i.e., that only acts as a detrend of the signal without corrupting its morphology; (3) whose efficiency does not depend on the experimenter's choices, i.e. that its application is completely data-driven; (4) whose efficiency does not depend on the characteristics of the EEG signal such as the number of electrodes. After the ADA correction, we observed that (1) the DA was completely removed and (2) the spatiotemporal distribution of the TMS-evoked activity was in agreement with previous studies. Specifically, in the time domain, the grand-averaged TEP waveforms after ADA correction showed the well-known pattern of TEPs, resulting in a sequence of positive and negative deflections, usually termed as P30, N45, P60, N100 and P180 (Paus et al., 2001; Kommsi et al., 2002; Bender et al., 2005; Bonato et al., 2006; Lioumis et al., 2009; Ferreri et al., 2011; Veniero et al., 2013; Casula et al., 2016b; 2017). Importantly, the TEP waveform morphology was entirely preserved after ADA correction, as

demonstrated by the results of experiment 1, which showed that none of the TEPs peak-to-peak amplitude differed from the original RAW signal. Moreover, the scalp maps and source reconstruction of the TMS-evoked activity showed the usual TEP distribution, i.e. the P30 focused in the site of stimulation; the N45 controlateral to the site of stimulation; the P60 distributed in the stimulated hemisphere; the N100 over the central areas of both hemispheres; and the P180 over the bilateral fronto-central areas (Bonato et al., 2006; Ferreri et al., 2011; Premoli et al., 2014; Casula et al., 2016b; 2017). Interestingly, we did not observe any difference in the TMS-evoked oscillatory activity among the three conditions. This confirms that the DA mainly affects the amplitude of the signal respect to the baseline but not the TEPs morphology *per se*.

In conclusion, the main contribution of this study is the proposal of a new adaptive algorithm for the correction of long-lasting artefacts induced by TMS during EEG. We demonstrated that ADA is a reliable solution for the DA correction, especially considering that (1) it does not affect physiological responses, since it only acts as an adaptive detrend of the signal; (2) it is independent from the experimenter's choices, since its application is completely data-driven and (3) its effectiveness is not dependent on the characteristics of the artefact and on the number of recording electrodes. We also showed the impact of the DA on different TMS-EEG measures, showing that it severely distorts the EEG signal in the time and in the space domain. Finally, we highlighted the limits of the common solutions proposed in literature, represented by linear detrend and ICA: on one hand, we showed the unsuitableness of the first method, being the DA mostly non-linear; on the other hand, we stressed the critical importance to establish standard and stable criteria of identification and removal of artefact-related ICA components, which are still lacking for TMS-EEG artefacts.

Conflict of interest

The authors declare that they have no conflict of interest.

Acknowledgements

We are grateful to Dr. Francesco Cecotti for his contribution on the development of the algorithm of correction. This study was partially supported by a grant from the Bial Foundation (84/12 to P. S. B.).

References

Akaike H (1979) *A new look at the statistical model identification.* IEEE Trans. Automat. Contr., 19:716-723

Bender S, Basseler K, Sebastian I, Resch F, Kammer T, Oelkers-Ax R, Weisbrod M (2005) *Transcranial Magnetic Stimulation Evokes Giant Inhibitory Potentials in Children*. Ann Neurol., 58:58-67

Bonato C, Miniussi C, Rossini PM (2006) *Transcranial magnetic stimulation and cortical evoked potentials: a TMS/EEG coregistration study*. Clin Neurophysiol., 117:1699-1707

Casula EP, Pellicciari MC, Picazio S, Caltagirone C, Koch G (2016a) *Spike-timing-dependent plasticity over the human dorsolateral prefrontal cortex.* NeuroImage, 143:204-213

Casula EP, Pellicciari MC, Ponzo V, Stampanoni Bassi M, Veniero D, Caltagirone C, Koch G (2016b) *Cerebellar theta burst stimulation modulates the neural activity of interconnected parietal and motor areas.* Sci Rep., doi:10.1038/srep36191

Casula EP, Stampanoni Bassi M, Pellicciari MC, Ponzo V, Veniero D, Peppe A, Brusa L, Stanzione P, Caltagirone C, Stefani A, Koch G (2017) *Subthalamic stimulation and levodopa modulate cortical reactivity in Parkinson's patients.* Parkinsonism Relat Disord., 34:31-37

Cobelli C, Foster D, Toffolo G (2000) *Tracer kinetics in biomedical research (vol. 1).* Springer Science & Business Media

Delorme A, Makeig S (2004) *EEGLAB: an open source toolbox for analysis of single-trial EEG dynamics including independent component analysis*. J Neurosci Methods., 134:9-21

Ferreri F, Pasqualetti P, Määttä S, Ponzo D, Ferrarelli F, Tononi G, Mervaala E, Miniussi C, Rossini PM (2011) *Human brain connectivity during single and paired pulse transcranial magnetic stimulation.* Neuroimage, 54:90–102

Hamidi M, Slagter HA, Tononi G, Postle BR (2010) *Brain responses evoked by high-frequency repetitive transcranial magnetic stimulation: An event-related potential study*. Brain Stimul., 3:2–14

Hernandez-Pavon JC, Metsomaa J, Mutanen T, Stenroos M, Mäki H, Ilmoniemi RJ, Sarvas J (2012) *Uncovering neural independent components from highly artefactual TMS-evoked EEG data.* J Neurosci Methods., 209:144-157

Ilmoniemi RJ e Kičić D (2010) *Methodology for Combined TMS and EEG.* Brain Topogr., 22:233-248

Ilmoniemi RJ, Virtanen J, Ruohonen J, Karhu J, Aronen HJ, Näätänen R, Toivo K (1997) *Neuronal responses to magnetic stimulation reveal cortical reactivity and connectivity*. Neuroreport, 8:3537-3540

Julkunen P, Pääkkönen A, Hukkanen T, Könönen M, Tiihonen P, Vanhatalo S, Karhu J (2008) *Efficient reduction of stimulus artefact in TMS–EEG by epithelial short- circuiting by mini-punctures*. Clin Neurophysiol., 119:475–481

Komssi S, Aronen HJ, Huttunen J, Kesäniemi M, Soinne L, Nikouline VV, Ollikainen M, Roine RO, Karhu J, Savolainen S, Ilmoniemi RJ (2002) *Ipsi- and contralateral EEG reactions to transcranial magnetic stimulation*. Clin Neurophysiol., 113:175–184

Komssi S, Kähkönen S, Ilmoniemi RJ (2004) *The effect of stimulus intensity on brain responses evoked by transcranial magnetic stimulation*. Hum Brain Mapp., 21:154–164

Korhonen RJ, Hernandez-Pavon JC, Metsomaa J, Mäki H, Ilmoniemi RJ, Sarvas J (2011) *Removal of large muscle artefacts from transcranial magnetic stimulation-evoked EEG by independent component analysis*. Med Biol Eng Comput., 49:397-407

Lehmann D and Skrandies W (1980) *Reference-free identification of components of checkerboard-evoked multichannel potential fields.* Electroencephalogr Clin Neurophysiol., 48: 609-621

Lioumis P, Kičić D, Savolainen P, Mäkelä JP, Kähkönen S (2009) *Reproducibility of TMS-Evoked EEG Responses*. Hum Brain Mapp., 30:1387-1396

Litvak V, Komssi S, Scherg M, Hoechstetter K, Classen J, Zaaroor M, Pratt H, Kähkönen S (2007) *Artefact correction and source analysis of early electroencephalographic responses evoked by transcranial magnetic stimulation over primary motor cortex.* Neuroimage, 37:56–70

Massimini M, Ferrarelli F, Huber R, Esser SK, Singh H, Tononi G (2005) *Breakdown of cortical effective connectivity during sleep*. Science, 309:2228–2232

Metsomaa J, Sarvas J, Ilmoniemi RJ (2014) *Multi-trial evoked EEG and independent component analysis*. J Neurosci Methods., 228:15-26

Mutanen T, Mäki H, Ilmoniemi RJ (2013) T*he effect of stimulus parameters on TMS-EEG muscle artefacts*. Brain Stimul., 6:371-376

Nikouline V, Ruohonen J, Ilmoniemi RJ (1999) *The role of the coil click in TMS assessed with simultaneous EEG.* Clin Neurophysiol., 110:1325-1328

Onton J, Westerfield M, Townsend J, Makeig S (2006) *Imaging human EEG dynamics using independent component analysis*. Neurosci Biobehav Rev., 30:808-822

Oostenveld R, Fries P, Maris E, Schoffelen JM (2011) *Fieldtrip: open source software for advanced analysis of MEG, EEG, and invasive electrophysiological data.* Comput Intell Neurosci., 2011:156869

Paus T, Castro-Alamancos MA, Petrides M (2001) *Cortico-cortical connectivity of the human mid-dorsolateral frontal cortex and its modulation by repetitive transcranial magnetic stimulation*. Eur J Neurosci., 14:1405-1411

Premoli I, Castellanos N, Rivolta D, Belardinelli P, Bajo R, Zipser C, Espenhahn S, Heidegger T, Müller-Dahlhaus F, Ziemann U (2014) *TMS-EEG Signatures of GABAergic Neurotransmission in the Human Cortex*. J Neurosci., 34:5603-5612

Rogasch NC, Thomson RG, Farzan F, Fitzgibbon BM, Bailey NW, Hernandez-Pavon JC, Daskalakis ZJ, Fitzgerald PB (2014) *Removing artefacts from TMS-EEG recordings using independent component analysis: Importance for assessing prefrontal and motor cortex network properties*. Neuroimage, 101:425-439

Rossi S, Hallett M, Rossini PM, Pascual-Leone A, The safety of TMS Consensus Group (2009) *Safety, ethical considerations, and application guidelines for the use of transcranial magnetic stimulation in clinical practice and research.* Clin Neurophysiol., 120:2008-2039

Sekiguchi H, Takeuchi S, Kadota H, Kohno Y, Nakajima Y (2011) *TMS-induced artefacts on EEG can be reduced by rearrangement of the electrode's lead wire before recording*. Clin Neurophysiol., 122:984-990

Ter Braack EM, De Jonge B, Van Putten MJ (2013) *Reduction of TMS induced artefacts in EEG using principal components analysis.* IEEE Trans Neural Syst Rehabil Eng., 21:376-382

Thut G, Northoff G, Ives JR, Kamitani Y, Pfennig A, Kampmann F et al. (2003) *Effects of single-pulse transcranial magnetic stimulation (TMS) on functional brain activity: a combined event-related TMS and evoked potential study*. Clin Neurophysiol., 114:2071-2080

Tiitinen H, Virtanen J, Ilmoniemi RJ, Kamppuri J, Ollikainen M, Ruohonen J, Näätänen R (1999) *Separation of contamination caused by coil clicks from responses elicited by transcranial magnetic stimulation*. Clin Neurophysiol., 110:982-985

Van Der Werf YD, Paus T (2006) *The neural response to transcranial magnetic stimulation of the human motor cortex. I. Intracortical and cortico-cortical contributions*. Exp Brain Res., 175:231-245

Veniero D, Bortoletto M, Miniussi C (2009) *TMS-EEG co-registration: On TMS-induced artefact*. Clin Neurophysiol., 120:1392-1399

Veniero D, Ponzo P, Koch G (2013) *Paired associative stimulation enforces the communication between interconnected areas*. J Neurosci., 33:13773-13783

Virtanen J, Ruohonen J, Naatanen R, Ilmoniemi RJ (1999) *Instrumentation for the measurement of electric brain responses to transcranial magnetic stimulation*. Med Biol Eng Comput., 37:322–326

Zanon M, Busan P, Monti F, Pizzolato G, Battaglini PP (2010) *Cortical connections between dorsal and ventral visual streams in humans: evidence by TMS/EEG co-registration.* Brain Topogr., 22:307-317

Figure legends

Figure 1

Grand-averaged TEP waveforms evoked from M1 stimulation in the four conditions: RAW (blue, panel A), ADA (red, panel B) INFOMAX (light green, panel C) and FASTICA (dark green, panel D). Above the panels is depicted the voltage distribution at -50 ms (baseline), 30, 45, 55, 100, 180 and 400 ms after the TMS pulse.

Figure 2

Cluster-based permutation analysis comparing TEPs in the RAW (blue line), INFOMAX (light green line, first column), FASTICA (dark green line; second column) and ADA condition (red line; fourth column). Black dots indicate the significant electrodes (*Monte Carlo p-values < 0.*01), black thick lines indicate the time windows detected as significant at the cluster-based permutation analysis (*Monte Carlo p-values < 0.01*).

Figure 3

TEPs peak-to-peak amplitude analysis comparing the RAW uncorrected data (blue bars) with the corrected data using ADA (red bars), INFOMAX (light green bars) and FASTICA (dark green bars). Asterisks indicate the significant differences between the conditions ($p < 0.05$).

Figure 4

Spatiotemporal distribution of some ICA components reflecting linear and non-linear trends of the DA evoked in the three areas of stimulation. The identification of the DA-related ICA components was based on their waveform and spatiotemporal distribution (methods section 2.3).

Figure 5

Spatiotemporal analysis of TMS-evoked activity from MFG stimulation in the RAW (blue) and ADA (red) condition. Three different analysis are depicted: TEPs recorded over all the scalp (above); GMFP (middle); maps of voltage distribution and cortical activity (below). Black dots indicate the electrodes detected as significant at the cluster-based permutation analysis (*Monte Carlo p-values < 0.01*).

Figure 6

Spatiotemporal analysis of TMS-evoked activity from M1 stimulation in the RAW (blue) and ADA (red) condition. Three different analysis are depicted: TEPs recorded over all the scalp (above); GMFP (middle); maps of voltage distribution and cortical activity (below). Black dots indicate the electrodes detected as significant at the cluster-based permutation analysis (*Monte Carlo p-values < 0.01*).

Figure 7

Time/space-domain analysis of TMS-evoked activity from IPS stimulation in the RAW (blue) and ADA (red) condition. Three different analysis are depicted: TEPs recorded over all the scalp (above); GMFP (middle); maps of voltage distribution and cortical activity (below). Black dots indicate the electrodes detected as significant at the cluster-based permutation analysis (*Monte Carlo p-values < 0.01*).

Figure 8

Time/frequency-domain analysis of TMS-evoked activity from MFG (above), M1 (middle) and IPS stimulation (below) in the RAW (blue) and ADA (red) condition. Wavelet plots depict the oscillatory activity from 4 to 50 Hz recorded in the electrodes closest to the site of stimulation (F3 for MFG, C3 for M1, P3 for IPS). Scalp maps depict the oscillatory activity recorded over all the scalp.